Numerical evaluation of heat transfer enhancement due to annular electroconvection induced by injection in a dielectric liquid

Jian Wu, Philippe Traoré and **Christophe Louste**
Institut PPRIME, Département Fluide-Thermique-Combustion
Boulevard Pierre et Marie Curie, BP 30179
86962 Futuroscope-Chasseneuil, France

and **Alberto T. Pérez**
Departamento de Electrónica y Electromagnetismo, Universidad de Sevilla
Facultad de Física, Avenida Reina Mercedes s/n
41012 Sevilla, Spain

and **Pedro A. Vázquez**
Departamento de Física Aplicada III, Universidad de Sevilla
ESI, Camino de los Descubrimientos s/n
41092 Sevilla, Spain

ABSTRACT

Two-dimensional numerical simulations are carried out to evaluate the enhancement of natural convection heat transfer in a dielectric liquid resulting from injection induced annular electro-convection. The liquid is confined between two concentric horizontal cylinders and subjected to the simultaneous actions of a direct current electric field and a thermal gradient. A unipolar injection from the inner cylinder introduces free space charges into the liquid. Numerical results are presented for the configuration of inner to outer diameter ratio of 0.5 and silicon oil as the working medium. It is found that the charge injection may induce a strong radial fluid motion, which consequently augments the heat transfer rate. Due to the linear stability nature of electro-convection, there exists a threshold value of the electric driving parameter, above which the electrical enhancement becomes manifest. In addition, when the electric driving parameter is sufficiently high, the flow is fully dominated by the Coulomb force, and thus heat transfer becomes independent of the thermal driving parameter.

Index Terms — **Electrohydrodynamics; dielectric liquid; charge injection; heat transfer enhancement; numerical analysis; annular geometry.**

1 INTRODUCTION

The electric field has been considered to actively enhance or control heat and mass transfer since a long time ago [1]. The prime motivation lies in that the electric-based techniques own some unique advantages, such as no moving parts, rapid and smart control, low power consumption, noise and pressure drop, and so on [2]. For single-phase liquids of low electrical conductivity, there are quite an amount of work considering different electrical forces to enhance convection and mixing, and thus heat transfer. On a fundamental level, three types of electrical body force can be distinguished when a fluid is subjected to an electric field [3],

$$\bar{f}_E = q\vec{E} - \frac{1}{2}E^2\nabla\varepsilon + \frac{1}{2}\nabla\left[\rho E^2\left(\frac{\partial\varepsilon}{\partial\rho}\right)_\theta\right] \quad (1)$$

where q is the free charge density, $\vec{E}$ the electric field, ε the permittivity of liquid, ρ the fluid density, and θ denotes the absolute temperature. The three terms on the right-hand side of Eqn. (1) represent, in order, the Coulomb force, the dielectric force and the electrostritive force. The Coulomb force is due to the electric field exerting on the non-negligible free space charges within the bulk liquid, and it generally dominates when a direct current (D.C.) electric field is imposed. The dielectric force requires the gradient of permittivity to be nonzero, which may be achieved by applying a thermal gradient across the liquid layer, assuming that the permittivity is temperate-dependent. It becomes important only when an alternating current (A.C.) electric field with a period much shorter than the charge relaxation time is present. The electrostrictive term is a gradient of a

scalar, so it can be combined within the fluid pressure.

Different mechanisms have been proposed to explain the sources of free space charges within dielectric liquids. For ohmic or quasi-ohmic liquids, these charges maybe come from a thermally induced conductivity gradient [4,5] or the field-enhanced dissociation (the Onsager effect) [6,7]. For liquids of very low conductivity, another mechanism referred as charge injection is more reasonable [8,9]. Ions are considered to be first generated due to the electrochemical reactions that take place at the interface between the liquid and the electrode surface. Depending on the polarity of the liquid and also the electrode material, all or part of the generated ions will enter into the bulk liquid under the action of the electric field. For a complete description the charge injection process, please refer to [10]. Experiments have demonstrated that ion injection is the predominant mechanism for the origination of free charges above the saturation voltage [11].

In this study, we consider a limit case of unipolar injection into a perfectly insulating liquid, which means only the Coulomb force is considered as the electrical force and the charge injection from one-side electrode serves as the source of free charges. This restricted model actually defines a lot of problems [10]. Most previous studies were concerned with the symmetrical geometry of parallel plates and the asymmetrical case of point/blade-plate; see the excellent review papers of [12,13]. From a practical application point of view, the configurations of concentric and eccentric cylinders are more interesting. The application examples include the electric transmission cables (such as the dielectric liquid- and air-filled pipe-type cables), vapor condensers, thermal energy storage systems, and so on [14].

Natural convection in concentric annuli, which is a fundamental problem in the thermal science field, has been extensively studied since 1960s. The up-to-date reviews of this topic can be found in [15, 16]. The heat transfer rate with natural convection in general is very low, especially in the regimes of conduction and transition [17]. The idea of this study is to impose an electric field on the thermal flows to enhance mixing and heat transfer within the fluid. Comparing to thermal convection, less work has been done with electro-convection in the cylindrical geometry. In addition, most of these studies are mainly concerned with the theoretical analysis with the linear instability of the problem [18,19,20]. There are some experimental studies concerning the heat transfer enhancement caused by the injection-induced convection in the annular geometry with forced flow (tubes or wire/cylinder) [21,22,23]. Significant increase in the heat transfer rate and slight increase with the pressure drop due to the imposed electric field was observed.

In two recent papers [24,25], we numerically studied the annular electro-convection of isothermal dielectric liquids induced by strong and weak charge injection. The subcritical bifurcation in the finite amplitude regime, a typical feature of electro-convection with symmetrically placed electrodes, is fully characterized. Here we extend the study to non-isothermal liquids. We will numerically evaluate the enhancement of natural convection heat transfer resulting from charge injection–induced electro-convection in a horizontal annulus. The remainder of the paper is organized as follows. In Section 2, we present the physical problem, governing equations and boundary conditions. In Section 3, the numerical methods are briefly described. Results and discussion are presented in Section 4. Finally, in Section 5, we summarize our findings.

2 PROBLEM FORMULATION

This section covers the description of the physical problem, the mathematical model, and the boundary and initial conditions.

2.1 PHYSICAL PROBLEM

We consider an insulating liquid layer lying between two infinite horizontal concentric circular cylinders. The radii of the inner and outer cylinders are denoted with R_i and R_o, respectively. The geometry of the problem and the Cartesian coordinate system used are depicted in Fig. 1.

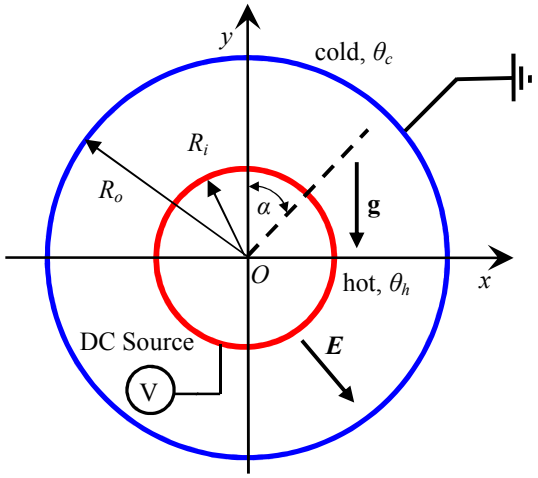

Figure 1. Sketch of electro-thermo-convection between two concentric circular cylinders with constant but different temperatures and electric potentials.

The two cylinders keep constant but different temperatures, θ_h and θ_c ($\theta_h > \theta_c$). A radial D.C. electric field is established by applying a voltage ΔV to the two electrodes. Only one species of homo-charges are injected from the inner cylinder, i.e. unipolar injection. To simplify the discussion, we adopted the *autonomous* and *homogeneous* assumption for injection, which means that the injected charge density at the emitter electrode q_0 is assumed to be constant and uniform [12,13]. This assumption is valid for the liquid subjected to a strong electric field in the range of $10^5 \le E \le 4\times10^6$ V/m [10]. The fluid of density ρ, kinematic viscosity ν, specific heat at constant pressure c_p, thermal expansion coefficient β, thermal diffusivity κ and permittivity ε, is assumed to be Newtonian and incompressible.

2.2 GOVERNING EQUATIONS

The governing equations include the mass conservation equation, the Navier–Stokes equations, the energy equation, a reduced set of Maxwell's equations, and together with some equations of state. Under the Boussinesq approximation, these equations can be written in the following dimensionless form

using the scales $H=R_o-R_i$, ΔV, $\varepsilon\Delta V/H^2$, ν/H and $\Delta\theta=\theta_h-\theta_c$ for, respectively, length, electric potential, charge density, fluid velocity and temperature [10,26],

$$\nabla\cdot\mathbf{v}=0 \tag{2}$$

$$\frac{\partial\mathbf{v}}{\partial t}+(\mathbf{v}\cdot\nabla)\mathbf{v}=-\nabla\hat{p}+\nabla^2\mathbf{v}+\frac{T^2}{M^2}Cq\mathbf{E}+\frac{Ra}{\mathrm{Pr}}\theta\mathbf{e}_y \tag{3}$$

$$\frac{\partial\theta}{\partial t}+\mathbf{v}\cdot\nabla\theta=\frac{1}{\mathrm{Pr}}\nabla^2\theta \tag{4}$$

$$\frac{\partial q}{\partial t}+\nabla\cdot\left[\left(\frac{T}{M^2}\mathbf{E}+\mathbf{v}\right)q\right]=0 \tag{5}$$

$$\nabla^2V=-Cq \tag{6}$$

$$\mathbf{E}=-\nabla V \tag{7}$$

where the vectors $\mathbf{v}\equiv[u,v]$, $\mathbf{E}\equiv[E_x,E_y]$ and $\mathbf{e}_y\equiv[0,1]$ denote the fluid velocity field, electric field and a unit direction vector in the y direction, respectively. The scalars q, V and θ stand for charge density, electric potential and temperature. The modified pressure $\hat{p}$ includes the dynamic pressure and the contribution from the electrostrictive force [16]. The last two terms in Eqn. (3) represent the Coulomb force and the buoyancy force.

Several simplifications and assumptions that are widely applied in modelling electrohydrodynamic flows of dielectric liquids are used in the above mathematical model. Since the electric current through the dielectric liquid is small, the magnetic effects and Joule heating are neglected. The molecular diffusion in the charge transport equation (5) is omitted because of its low contribution comparing to convection and drift [27]. The dielectric permittivity ε and ionic mobility K are assumed to be constant, independent on temperature and electric field.

Five dimensionless numbers defined as follows appear in above equations,

$$Ra=\frac{g\beta\Delta\theta H^3}{\kappa\nu},\quad Pr=\frac{\nu}{\kappa\nu},$$

$$T=\frac{\varepsilon\Delta V}{\rho\nu K},\quad C=\frac{q_0H^2}{\varepsilon\Delta V},\quad M=\frac{1}{K}\left(\frac{\varepsilon}{\rho}\right)^{1/2},$$

where g is the gravity acceleration. The Rayleigh number Ra and the electric Rayleigh number T are defined as the ratios of the buoyancy force and Coulomb force to the viscous force, respectively. Ra and T can be viewed as the dimensionless temperature difference and voltage. Pr stands for the Prandtl number. The mobility number M is defined as the ratio between the hydrodynamic mobility to the ionic mobility. Both Pr and M are solely decided by the properties of liquid. The injection parameter C measures the injection strength. The problem also depends on the radius ratio, which is a geometry-related parameter and it is defined as $\Gamma = R_i/R_o$ ($\Gamma<1$). To show the heat transfer rate, the local Nusselt numbers are defined on the inner and outer cylinders as,

$$Nu_i=R_i\ln\left(\frac{R_o}{R_i}\right)\left.\frac{\partial\theta}{\partial r}\right|_{r=R_i},\quad Nu_o=R_o\ln\left(\frac{R_o}{R_i}\right)\left.\frac{\partial\theta}{\partial r}\right|_{r=R_o},$$

where $\partial\theta/\partial r$ is the temperature gradient in the radial direction. The mean Nusselt number on each cylinder is computed by integration,

$$\overline{Nu_i}=\frac{1}{2\pi}\int_0^{2\pi}Nu_i(\alpha)d\alpha,\quad \overline{Nu_o}=\frac{1}{2\pi}\int_0^{2\pi}Nu_o(\alpha)d\alpha.$$

Because of the energy conservation law, the values of $\overline{Nu_i}$ and $\overline{Nu_o}$ should be equal to each other. Slight difference may be induced by the numerical methods, so the final mean Nusselt number is calculated as the average value of $\overline{Nu_i}$ and $\overline{Nu_o}$, i.e. $\overline{Nu}=\left(\overline{Nu_i}+\overline{Nu_i}\right)/2$.

2.3 BOUNDARY AND INITIAL CONDITIONS

The non-dimensional computational domain is defined by the annulus $\Gamma/(1-\Gamma)\le r\le 1/(1-\Gamma)$ and $0\le\alpha\le 2\pi$. The no-slip condition for fluid velocity ($u=v=0$) is imposed on the two cylinders. Other boundary conditions include:

inner cylinder ($r=R_i$): $V=1$, $q=1$, $\theta=1$;

outer cylinder ($r=R_o$): $V=0$, $\theta=0$.

Since Eqn.(5) is first-order hyperbolic, no physical boundary condition for q is required at the outer cylinder [28]. The zero-field for all variables serves as the initial condition.

3 NUMERICAL METHODS

The numerical procedure is based on a full and direct integration of Eqns. (2)-(7) with a 2nd order finite volume method [29]. A boundary-fitted structured grid that consists of nonorthogonal quadrilaterals is used to discretize the computational domain. Fig. 2 shows an example of discretized grid. The grid is uniform in the axial direction and strongly non-uniform in the radial direction. The finer grid size close to the inner cylinder aims to capture the sharp gradient of charge density within this region [24]. A collocated arrangement is adopted, which means all variables are stored at the center of each quadrilateral mesh.

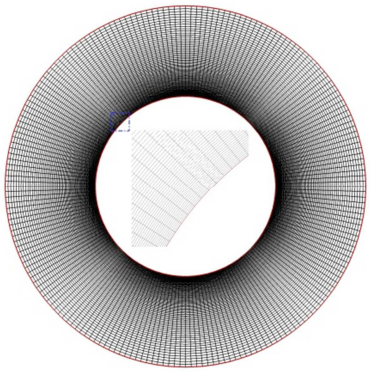

Figure 2. An example of discretized grid consisting of structured quadrilateral meshes.

For the Navier-Stokes equations, both convective and diffusive fluxes are computed with the central differencing scheme. The semi-implicit three time levels scheme [29] is used for time integration. The SIMPLE algorithm [30] is undertaken to couple the fluid velocity and pressure, and the Rhie-Chow algorithm [31] is implemented for momentum interpolation. The algorithms for the temperature equation (4)

and electrostatics equations (5)-(7) are explained in detail in [32]. The Smooth Monotonic Algorithm for Real Transport (SMART) scheme [33] is especially applied to the hyperbolic equation (5), aiming at preventing unphysical oscillations and at the same time reducing numerical diffusion. A detailed description of the complete computation procedure and the nonlinear couplings between charges, temperature, fluid velocity field and electric field can be found in [34].

4 RESULTS AND DISCUSSION

We consider the silicon oil that was used in the experimental studies [35] as the working liquid. The values of Pr and M corresponding to this liquid are 116.6 and 49.0, respectively. The injection strength is considered to be strong, C=10. A representative case of the radius ratio, Γ=0.5, is treated. The dimensionless radii of the inner and outer cylinders are 1.0 and 2.0, respectively. All numerical results are obtained with a grid of 450×150 control volumes (CVs). This grid is finally selected based on extensive grid-independent tests. Computations of pure thermal- and electro-convection are first performed to validate our numerical algorithm, and to highlight the difference between the two types of flows.

4.1 NATURAL CONVECTION

Computations are performed to simulate natural convection without any electrical effect. To validate the thermal module of our numerical solver, the benchmark case with Pr = 0.706, Γ= 0.3846 and Ra = 4.7×10^4 is considered, and the experimental results of Kuehn and Goldstein [14] are used for comparison. Our numerically obtained isotherms and the experimental results are presented in Fig. 3a and Fig. 3b, respectively. A quantitative comparison can be found in Fig. 4, in which the distribution of radial temperature and the local equivalent thermal conductivity (defined as the ratio between the local Nusselt number and the Nusselt number assuming pure heat conduction) are plotted. As shown in Fig. 3 and Fig. 4, our numerical results are in a fairly good agreement with the experimental data.

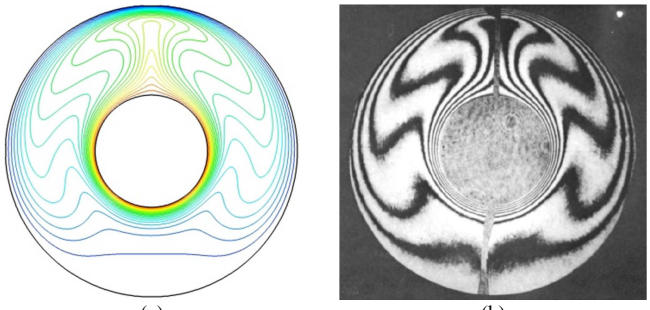

(a) (b)

Figure 3. Comparison of isotherms for Pr=0.706, Γ=0.3846 and Ra=4.7×10^4 between (a) our numerical result and (b) the experimental result of Kuehn and Goldstein [14].

We now consider the natural convection with the annulus of Γ=0.5, Pr=116.6 and four different values of Ra (=10^2, 10^3, 10^4, and 10^5). Because of the lack of available results with the same values of parameters considered, our results have been compared with the ones obtained with a Lattice Boltzmann method [36] for verification. The distributions of temperature (left) and the lines of constant stream function (right) are presented in Fig. 5. Since the figures with Ra=10^2 are very similar to the ones of Ra=10^3, they are not provided.

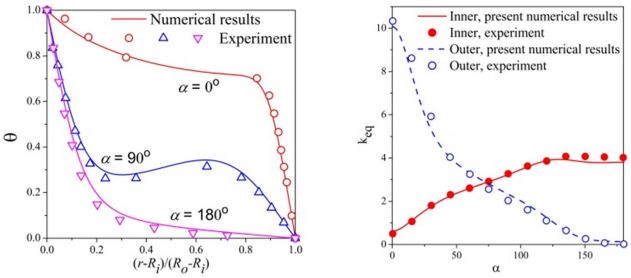

(a) (b)

Figure 4. Comparison of (a) the radial temperature distribution and (b) the local equivalent conductivity between our numerical result and the experimental result of Kuehn and Goldstein [14].

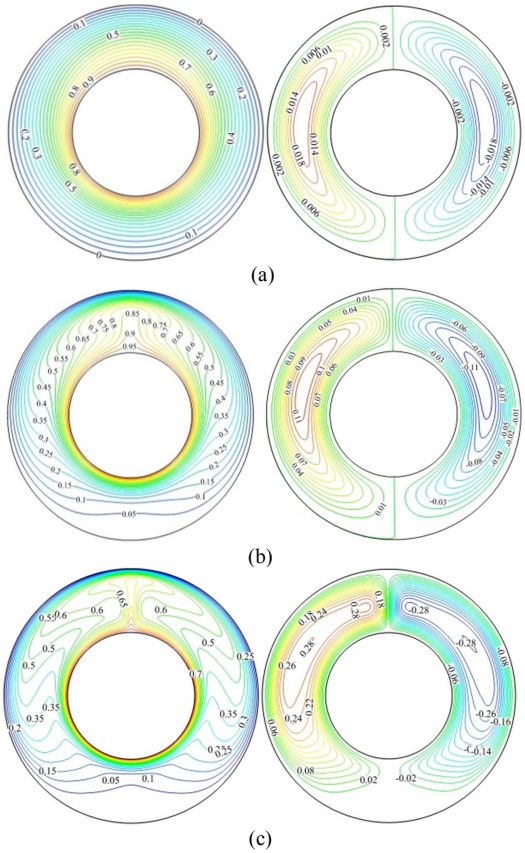

(a) (b) (c)

Figure 5. Distributions of temperature (left) and stream function (right) for nature convection with Pr=116.6, Γ=0.5, (a) Ra=10^3, (b) Ra=10^4, (c) Ra=10^5.

Unlike the Rayleigh-Bénard convection of a horizontal fluid layer heated from below, which requires a high enough temperature difference to induce fluid motion, even a small temperature difference in the cylindrical configuration can result in convection. For all values of Ra considered, the flow pattern is steady with two recirculation cells symmetrically locating to the vertical line x = 0. We also tried some higher Rayleigh numbers ($Ra \geq 10^6$) and observed unsteady flow patterns. For low values of Ra, the convection is very weak, and the flow pattern as well as heat transfer is conduction-

dominated. As it can be seen from Fig. 5, the isotherms resemble quasi-eccentric circles and the maximum stream function (i.e. the center of rotation) is near the position of α = 90°. The top and bottom portions of the annulus is almost symmetrical with respect to the horizontal line y = 0. At the opposite limit, for high values of *Ra*, the flow is of boundary layer type [37] and the isotherms greatly change. Two thin boundary layers are fully developed around the inner and outer cylinders; see Fig. 5c. There is a buoyant plume above the inner cylinder locating at top region and impinging towards the outer cylinder. With increasing *Ra* values, the center of rotations move closer to the line of symmetry, x = 0. Fig. 5b shows an example of the intermediate region (named as the transition region [15]) between the pseudo-conduction and the boundary layer regimes.

Table 1 summarizes the average Nusselt numbers for natural convection. These values will be used as the references to quantify the effect of electrical enhancement. We notice that for $Ra \le 10^3$ the contribution of convection to heat transfer is very limited.

Table 1. Average Nusselt Numbers for Natural Convection with Pr=116.6 and Γ=0.5.

Ra	10^2	10^3	10^4	10^5
$\overline{Nu_i}$	1.00040	1.05219	1.91546	3.36250
$\overline{Nu_o}$	1.00042	1.05212	1.91375	3.35359
$\overline{Nu}$	1.00041	1.05216	1.91461	3.35805

4.2 ELECTRO-CONVECTION

The *homogeneous* and *autonomous* injection induced dielectric flows in configurations of symmetrically placed electrodes (such as two parallel plates, concentric cylinders and spheres) possess a hydrostatic state, which means the fluid keeps still while charges are transported only by the electric field. The hydrostatic solution for the case of concentric cylinders may be expressed as [19, 24],

$$u = v = 0\,,\ q_s(r) = \frac{a}{C\sqrt{r^2 + B}}\,,\ E_s(r) = \frac{A}{r}\sqrt{r^2 + b}\,, \qquad (8)$$

where a and b are two constants depending on C and Γ. For C=10 and Γ=0.5, a and b are 1.439 and -0.979 respectively. In Figure 6 we have displayed the numerically obtained hydrostatic solutions. An excellent agreement between numerical and analytical results is shown. As shown in Fig. 6b, most charges concentrate at the region close to the inner cylinder, and the profile of charge density shows a sharp variation in this region.

The above described hydrostatic state is potentially unstable. That is, when the driving parameter T is greater than a critical value, the Coulomb force is strong enough to overcome the viscous damping and the flow motion arises (i.e. electro-convection). This threshold value can be accurately predicted by the linear stability analysis approach. It is reported that the stability criterion is dependent on the injection strength, the injection direction (from inner or outer cylinder) and the radius ratio, independent on the mobility number [18,19]. For the case we considered (two dimensions, inner injection, C=10, Γ=0.5), the critical T value (marked as T_c) and the associated critical wave number m_c are 122.54 and 7, respectively [24].

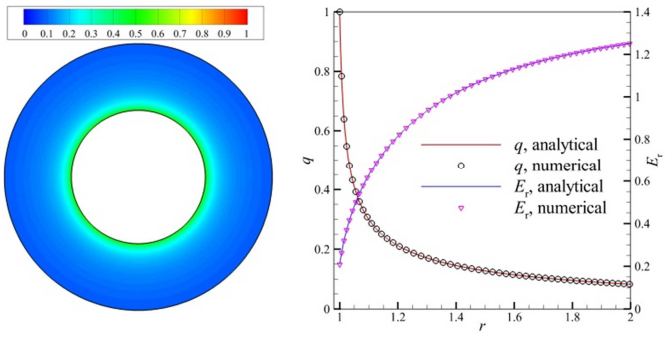

(a) (b)

Figure 6. (a) Charge density distribution in the hydrostatic state, (b) comparison between analytical and numerical profiles of hydrostatic state.

In Fig. 7 we have displayed the charge density and stream function isocontours for T=135, a value slightly higher than T_c. A steady fluid motion with well-organized structure is readily seen. The flow shows itself in a very different structure from that of natural convection. Seven pairs of counter-rotating vortexes are observed in Fig. 7b. The number of vortexes is decided by the critical wave number m_c. In Fig. 7a, we notice that there are seven discrete regions which are almost free of charges ($q \to 0$). Such charge-free region is formed due to the competition between the electric field and the fluid velocity field, and it is a very characteristic feature of Coulomb-driven convection. A detailed discussion with the flow structure can be found in [24]. We have also determined T_c from our direct numerical results and obtained T_c=122.61, which is very close to the analytical value 122.54.

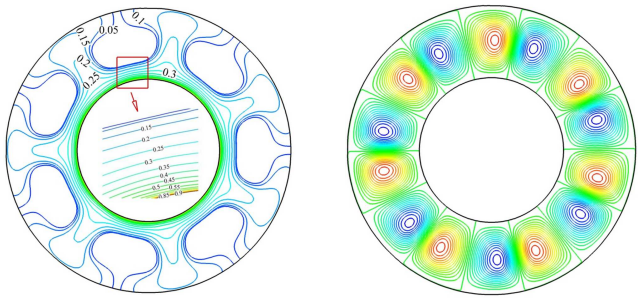

(a) (b)

Figure 7. Solutions of pure electro-convection for T=135, M=49 and Γ=0.5, (a) charge density (b) stream function.

Along with the increase in T, the strength of motion also gradually increases. In addition, some nonlinear instability takes places. We have carried out computations for a wide range of T (from 0 up to 1000). The flow pattern goes through such a transition: hydrostatic state (S1) → steady convective state with 7 pairs of vortexes (S2) → steady convective state with 8 pairs of vortexes; see Fig. 8a (S3) → oscillatory state (S4) → chaotic state (S5). Similar routes to chaos have also been revealed by Fernandes et al., [38]. The transition from S1 to S2 happens at T_c =122.54, from S2 to S3 at $T \approx 210$, and from S3 to S4 at $T \approx 350$. For $T \ge 500$, the flow enters into the chaotic regime. In this regime, dramatic fluctuations in the charge density field and the fluid velocity field are accompanied by the appearance of electro-plumes. The

electro-plumes are essentially a local structure of charges. They are randomly and intermittently generated within the charge density layer near the emitter electrode; see Fig. 8b. Electro-plume shares strong analogy with the thermal plume of Rayleigh-Bénard convection [39]. Such an electro-plume phenomenon has also been observed in the plate-plate configuration [40].

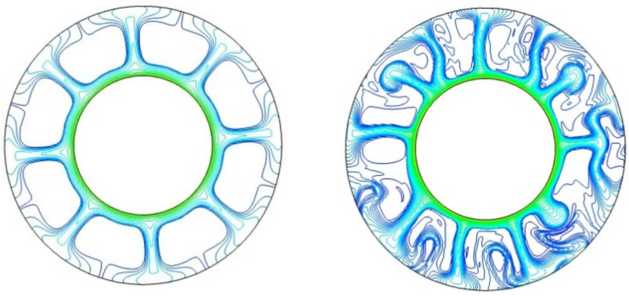

(a) (b)

Figure 8. Charge density distribution for (a) T=300, (b) T=500, a snapshot to highlight the electro-plumes.

4.3 HEAT TRANSFER ENHANCEMENT

Now we study the heat transfer enhancement due to charge injection. A two-step procedure is adopted. First, we run the computation of natural convection. After the steady state of thermal convection is reached, the electric field as well as charge injection is imposed. Then the liquid is under the simultaneous actions of buoyancy force and Coulomb force. For each case, we gradually vary T in a wide range. Experimentally, this procedure can be achieved by first applying the temperature difference, and then adding the applied voltage and adjusting it step by step.

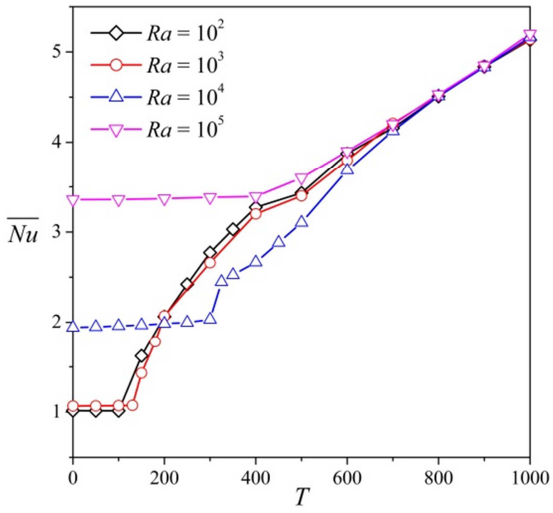

Figure 9. Mean Nusselt numbers $\overline{Nu}$ versus T for different Ra values. For unsteady flows, $\overline{Nu}$ were computed as the average value over a sufficiently long period of time.

In Fig. 9 we have summarized the variation of the mean Nusselt number with T for four Ra values considered. The first interesting finding is the existence of an obvious transition (denoted the corresponding T value as T_t) along each curve. For $T<T_t$, the increase of $\overline{Nu}$ with T is negligible. By checking the fluid velocity field, we find that the flow shows the same structure as pure thermal convection, i.e. two large "crescent" cells. The imposed electric field and injected charges have almost no impact on the temperature distribution, while the charge density distribution is strongly affected by the recirculation induced by the buoyancy force. In Fig. 10 we have provided two limiting examples within the regimes of $T<T_t$. For a small Ra (for example, $Ra=10^2$), the strength of buoyancy force and is weak, and thus the intensity of fluid motion is also weak. In this case, heat and charges are mainly transported by diffusion and ion drift, respectively. As it can be seen in Fig. 10a, the temperature profile approaches the result of pure heat conduction while the charge density profile approaches the hydrostatic solution. The thermal field and the electric field can be approximately considered as uncoupled. At the opposite limit with a high Ra value (for example, $Ra=10^5$), the strength of fluid motion induced by a large buoyancy force is strong. In this case, charge density can be viewed as a passive scalar, and its distribution is controlled by the fluid circulation. This explains why charges concentrate in the inner and outer boundary layers in Fig. 10b(ii).

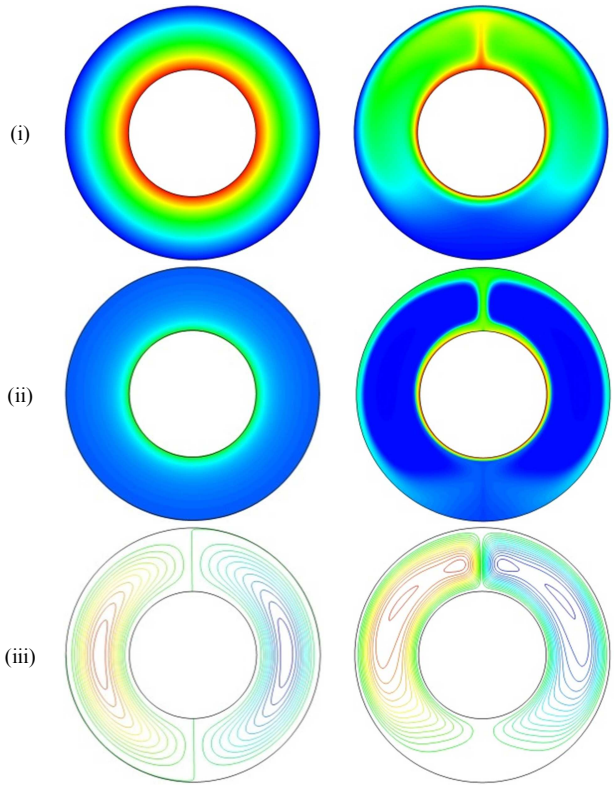

Figure 10. Two cases showing that charge injection has negligible effect on the flow motion, T = 100, (a) $Ra = 10^2$, (b) $Ra = 10^5$. (i) temperature, (ii) charge density, and (iii) stream function.

For $T>T_t$, the injected charges successfully induce radial secondary motions. More convective cells arise, and thus mixing and heat transfer is enhanced. As shown in Fig.9, the heat transfer rate in this second regime quickly increases as T increases. The distributions of both temperature and charge density are significantly affected by the injection induced secondary flows. We highlight that the value of T_t and the

flow patterns in this second regime are closely related to *Ra*. A large *Ra* value corresponds to a high T_t. For $Ra = 10^2$, 10^3, 10^4, and 10^5, T_t values are about 125, 135, 290 and 400, respectively. For small *Ra* values, T_t tends to T_c. This is because radial flows arise more easily with uniformly distributed charge density field.

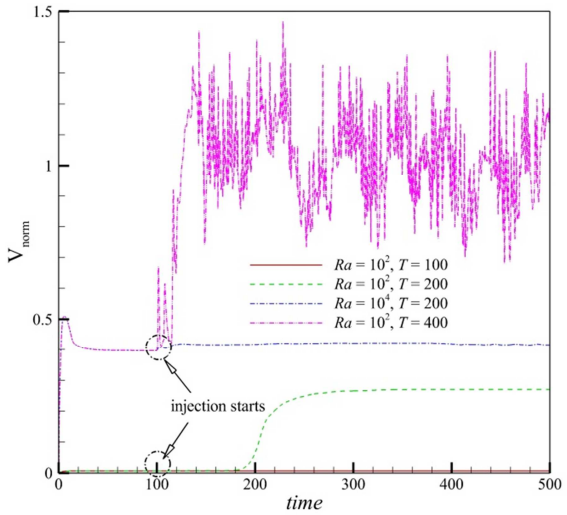

Figure 11. Temporal evolution of the maximum velocity norm V_{norm}. Charge injection starts at *time* = 100.

In Fig.11 we have plotted the time evolution of the maximum velocity norm V_{norm} defined as $V_{norm} = \max\left[\sqrt{u^2 + v^2}\right]$ for four representative cases investigated. Charge injection always takes place at *time* = 100. For (Ra=10^2, T=100) and (Ra=10^4, T=200), the radial secondary flow does not appear, and V_{norm} only slightly increases. For (Ra=10^2, T=200), a steady convection with 7 pairs of counter-routing vortices is formed at the end; see Fig. 12a. Before that, there is a slowly growing stage (from *time* = 100 to 250). The final charge density distribution and fluid velocity field share strong analogy with the case of pure electro-convection (comparing Fig.12a to Fig.7). In this case, heat can be viewed as a passive scalar. The increase in the number of convective cells substantially increases heat transfer.

For (Ra=10^4, T=400), the formation and the final pattern of flow is more complicated. Since the buoyancy force and the Coulomb force with this case are of the same order, the thermal field, flow field, electric field and charges are strongly coupled, which leads to a very irregular motion. As shown in Fig.11 that once charge injection starts, the radial secondary flow arises soon. After a short adjustment period, the flow enters into a quasi-periodic regime. By carefully examine the flow field we find that the radial convection always starts at the top region of the annulus (i.e. the region with the upward thermal plume and most injected charges), and then affects other region by the global circulation. In Fig. 12b we present a snapshot of the temperature, charge density and stream function isocontours to highlight the irregularity of flow. Comparing to $Ra = 10^2$, less convective cells are formed in the case of $Ra = 10^4$; see Fig. 12(iii). This explains why the $\overline{Nu}$ curve of $Ra = 10^4$ in Fig. 9 is lower than the ones of $Ra = 10^2$ and 10^3 in a wide range of T.

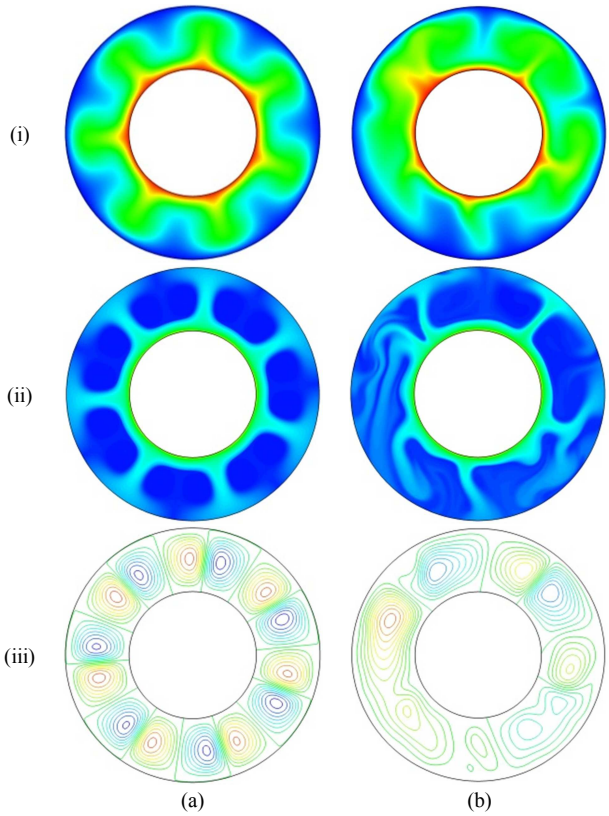

Figure 12. Two cases showing that charge injection has significant effect on the flow and heat transfer, (a) $Ra = 10^2$, $T = 200$ (b) $Ra = 10^4$, $T = 400$. (i) temperature, (ii) charge density, and (iii) stream function.

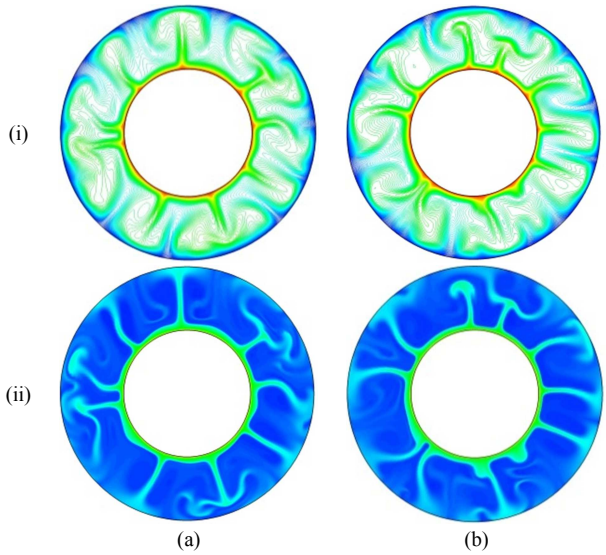

Figure 13. Snapshots of distributions of (i) temperature and (ii) charge density with the same high T value, $T = 1000$, (a) $Ra = 10^2$ and (b) $Ra = 10^4$.

We notice in Fig. 9 that $\overline{Nu}$ becomes independent on *Ra* for high T values. For example, at $T = 1000$, the values of $\overline{Nu}$ for $Ra = 10^2$ and 10^4 are 5.133 and 5.165, respectively. This is because the flows with sufficiently high T values are fully dominated by the Coulomb force. In Fig. 13 we have provided two snapshots of the distributions of temperature and charge density for two different *Ra* values ($Ra = 10^2$ and 10^4) with a

same high T value (T=1000). First, electro-plumes are generated over the whole inner cylinder in both cases, which indirectly proves that the buoyancy force no longer plays an important role. Otherwise, more plumes will be generated at the top region of the annulus. Second, we notice that in each case the positions and shapes of thermal plumes are almost exactly the same as of electro-plumes, which means heat is entrained as a passive scalar by the motion induced by charge injection. Note that the weak dependence of $\overline{Nu}$ on Ra at high T values has been observed experimentally [35,41] and numerically [26,34] in the plate-plate configuration.

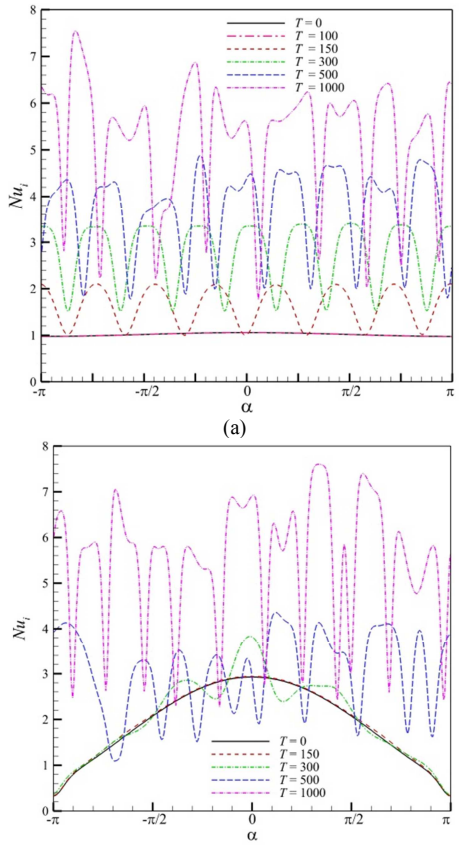

Figure 14. Local Nusselt number variation along the inner cylinder for (a) Ra = 10^2 and (b) Ra = 10^4 with various T values.

In Fig.14 we have plotted the local Nusselt number distribution along the inner cylinder for Ra=10^2 and 10^4 with various T values. The previous analysis with the flow patterns and their relationship with Ra and T can be further confirmed from Fig. 14. For Ra=10^2, the Nu_i curve of natural convection (i.e. T=0) takes a constant value 1.0, which indicates that heat is almost completely transferred via conduction. Slightly increasing T to 100, a value smaller than T_t (about 125), the flow pattern does not change, and the resulting Nu_i curve coincides with the curve of T=0. When T is increased above T_t, radial convection arises, and consequently the distribution of Nu_i dramatically changes. For T =150 and 300, we read from the flow field that there are 7 and 8 pairs of counter-rotating cells, respectively. This is directly reflected by the number of humps with Nu_i curves in Fig. 12a. Note that the number of convective cells with electro-thermo-convection (Ra=10^2 and T=150, 300) is the same as pure electro-convection; see Fig. 7 and Fig. 8a. In addition, the sudden increase in the number of convective cells leads to the non-smoothness of $\overline{Nu}$ curve (Fig. 9) in the range of $T > T_t$. By further increasing T, the flow becomes chaotic, which leads to an very irregular distribution of Nu_i.

For Ra = 10^4, the Nu_i curve of natural convection shows an upward hump in the central region (i.e. around α = 0), at where the thermal plume is generated. Since for this Ra value the value of T_t is about 290, radial convection does not appear for T = 150 ($<T_t$), and thus the curve of T = 150 in Fig. 14b is undistinguishable from the curve of T = 0. For T = 300, there is radial convection. However, due to the influence of buoyancy force, the radial convection only appears in the top region of the annulus, which is manifested by the upward and downward humps in the range of [-π/2, π/2]. Even higher T values lead to stronger radial flows covering the whole annulus [-π, π]. We notice that the number of humps and the maximum value of Nu_i with the curves of T = 1000 in Fig. 14a and 14b are close to each other. This again highlights the flow fields are entirely determined by the Coulomb force, while the buoyancy force plays a minor role.

5 CONCLUSIONS

A direct current electric field is considered to actively enhance nature convection heat transfer in a dielectric liquid lying between two concentric horizontal circular cylinders. Free charges are considered to be from unipolar injection. An in-house numerical solver based on the finite volume method is developed to solve all governing equations including a reduced set of Maxwell's equations, the Navier-Stokes equations and the energy equation. Numerical results are presented for an annulus with the ratio of inner to outer diameter of 0.5 and with silicon oil as the working liquid. The injection is considered to be strong and from the inner cylinder. Several Rayleigh numbers Ra ($10^2 \le Ra \le 10^5$) which represent different strengths of the buoyancy force are investigated. It is found that heat transfer can be effectively augmented by the radial flow motion induced by the Coulomb force for all Ra values considered. However, there exists a critical value of the electric driving parameter T (marked as T_t), only above which the electrical enhancement becomes to emerge. Such a phenomenon is essentially related to the linear stability nature of pure electro-convection with symmetrically placed electrodes. In addition, we find that the value of T_t increases as Ra increases. For small Ra, T_t tends to the linear stability criterion of pure electro-convection. Finally, for sufficiently high T values, the flow is fully dominated by the Coulomb force, and thus the heat transfer rate becomes independent on Ra.

ACKNOWLEDGMENT

This work was partially funded by the French Government program "Investissements d'Avenir" (LABEX INTERACTIFS, reference ANR-11-LABX-0017-01) (to Jian Wu), a grant of the French district Poitou- Charentes (to P. Traoré), and partially by financial support from the Spanish Ministerio de Cienciay Tecnología (MCYT) under Research Project No. FIS2011-25161 and Junta de Andalucía under research projects P10-FQM-5735 and P09-FQM-4584 (to A. T. Pérez). Jian Wu thanks to Professor H. L. Yi of Harbin Institute of Technology for his reference results of natural convection obtained with the Lattice Boltzmann method.

REFERENCES

[1] T. B. Jones, "Electrohydrodynamically enhanced heat transfer in liquids - A review", *Adv. Heat Transfer*, 14, 107-148, 1978.

[2] J. Seyed-Yagoobi, J. E. Bryan, "Enhancement of heat transfer and mass transport in single-phase and two-phase flows with electrohydrodynamics", *Adv. Heat Transfer*, 33, 95-186, 1999.

[3] L. M. Landau, E. M. Lifshitz, Electrodynamics of Continuous Media, Addison-Wesley, Reading, Mass., 1971.

[4] M. J. Gross, J. E. Porter, "Electrically induced convection in dielectric liquids", *Nature*, 1343-1345, 1966.

[5] P. J. Martin, A. T. Richardson, "Conductivity models of electrothermal convection in a plane layer of dielectric liquid", *J. Heat Transfer*, 106(1), 131-136, 1984.

[6] L. Onsager, "Deviations from Ohm's law in weak electrolytes", *J. Chem. Phys.*, 2(9), 599-615, 1934.

[7] J. C. Ryu, H. J. Park, J. K. Park, K. H. Kang, "New electro-hydrodynamic flow caused by the Onsager effect", *Phys. Rev. Lett.*, 104(10), 104502, 2010.

[8] N. Felici, "DC Conduction in liquid dielectrics: a survey of recent progress (Part I)", *Direct Current*, 2(3), 90-99, 1971.

[9] A. Denat, B. Gosse, J. P. Gosse, "Ion injections in hydrocarbons", *J. Electrostat.*, 7, 205-225, 1979.

[10] A. Castellanos (Eds.), "Electrohydrodynamics", Springer, New York, 27-31, 1998.

[11] A. Denat, B. Gosse, J. P. Gosse, "High field DC and AC conductivity of electrolyte solutions in hydrocarbons", *J. Electrostat.*, 11(3), 179-194, 1982.

[12] A. Castellanos, "Coulomb-driven convection in electrohydrodynamics", *IEEE Trans. Electrical Insulation*, 26 (6), 1201-1215, 1991.

[13] P. Atten, "Electrohydrodynamic instability and motion induced by injected space charge in insulating liquids", *IEEE Trans. Dielectrics and Electrical Insulation*, 3(1), 1-17, 1996.

[14] T. H. Kuehn, R. J. Goldstein, "An experimental and theoretical study of natural convection in the annulus between horizontal concentric cylinders", *J. Fluid Mech.*, 74(04), 695-719, 1976.

[15] D. Angeli, G. S. Barozzi, M. W. Collins, et al, "A critical review of buoyancy-induced flow transitions in horizontal annuli", *Int. J. Therm. Sci.*, 49(12), 2231-2241, 2010.

[16] H. Togun, T. Abdulrazzaq, S. N. Kazi, et al., "A review of studies on forced, natural and mixed heat transfer to fluid and nanofluid flow in an annular passage", *Renew. Sust. Energ. Rev.,* 39, 835-856, 2014.

[17] P. Teertstra, M. M. Yovanovich, "Comprehensive review of natural convection in horizontal circular annuli". *ASME-Publications-HTD*, 357, 141-152, 1998.

[18] A. T. Richardson, "The linear instability of a dielectric liquid contained in a cylindrical annulus and subjected to unipolar charge injection", *Q. J. Mech. Appl. Math.,* 33(3), 277-292, 1980.

[19] N. Agrät, A. Castellanos, "Linear convective patterns in cylindrical geometry for unipolar injection", *Phys. Fluids,* 2(1), 37-44, 1990.

[20] D. V. Fernandes, H. D. Lee, S. Park, Y. K. Suh, "Electrohydrodynamic instability of dielectric liquid between concentric circular cylinders subjected to unipolar charge injection", *J. Mech. Sci. Tech.,* 27(2), 461-467, 2013.

[21] J. Fernández, R. Poulter, "Radial mass flow in electrohydrodynamically-enhanced forced heat transfer in tubes", *Int. J. Heat Mass Transfer*, 30(10), 2125-2136, 1987.

[22] P. Atten, L. Elouadie, B. Malraison, "Electro-convection in a wire-cylinder geometry with forced flow and its effect on heat transfer", *IEEE Ind. Appl. Soc. Annual Meeting*, 2078-2083, 1989.

[23] P. Atten, L. Elouadie, "EHD convection in a dielectric liquid subjected to unipolar injection: coaxial wire/cylinder geometry", *J. Electrostat.*, 34(2), 279-297, 1995.

[24] J. Wu, P. A. Vázquez, P. Traoré, A. T. Pérez, "Finite amplitude electroconvection induced by strong unipolar injection between two coaxial cylinders", *Phys. Fluids,* 26(12), 124105, 2014.

[25] J. Wu, P. Traoré, P. A. Vázquez, A. T. Pérez, "Numerical simulation of annular electroconvection in a dielectric liquid induced by unipolar injection", *IEEE 18th Int. Conf. on Dielectric Liquids (ICDL)*, 2014.

[26] P. Traoré, A. T. Pérez, D. Koulova, H. Romat, "Numerical modeling of finite-amplitude electro-thermo-convection in a dielectric liquid layer subjected to both unipolar injection and temperature gradient", *J. Fluid Mech.*, 658(1), 279-293, 2010.

[27] A. T. Pérez, A. Castellanos, "Role of charge diffusion in finite amplitude electro-convection", *Phys. Rev. A*, 40(10), 5844-5855, 1989.

[28] R. J. LeVeque, Finite Volume Methods for Hyperbolic Problems, Cambridge, U.K.: Cambridge Univ. Press, 129, 2004.

[29] J. H. Ferziger, M. Perić, Computational Methods for Fluid Dynamics, 3rd ed., Springer, NewYork, 2002.

[30] S. V. Patankar, D. B. Spalding, "A calculation procedure for heat, mass and momentum transfer in three-dimensional parabolic flows", *Int. J. Heat Mass Transfer*, 15(10), 1787-1806, 1972.

[31] C. M. Rhie, W. L. Chow, "Numerical study of the turbulent flow past an airfoil with trailing edge separation", *AIAA J.*, 21(11), 1525–1532, 1983.

[32] J. Wu, P. Traoré, C. Louste, "An efficient finite volume method for electric field–space charge coupled problems", *J. Electrostat.*, 71(3), 319-325, 2013.

[33] P. H. Gaskell, A. K. C. Lau, "Curvature- compensated convective transport: SMART, a new boundedness-preserving transport algorithm", *Int. J. Numer. Meth. Fluids*, vol. 8(6), 617-641, 1988.

[34] J. Wu, P. Traoré, A finite-volume method for electro-thermoconvective phenomena in a plane layer of dielectric liquid, *Num. Heat Transfer-Part A,* 68, 1-30, 2015.

[35] F. M. J. McCluskey, P. Atten, A. T. Pérez, "Heat transfer enhancement by electroconvection resulting from an injected space charge between parallel plates", *Int. J. Heat Mass Transfer*, 34(9), 2237-2250, 1991.

[36] K. Luo, H. L. Yi, H. P. Tan. "Eccentricity effect on bifurcation and dual solutions in transient natural convection in a horizontal annulus", *Int. J. Therm. Sci.*, 89, 283-293, 2015.

[37] M. C. Jischke, M. Farshchi, "Boundary layer regime for laminar free convection between horizontal circular cylinders", *J. Heat Transfer*, 102(2), 228-235, 1980.

[38] D. V. Fernandes, H. D. Lee, S. Park, Y. K. Suh, "Numerical simulation of the electro-convective onset and complex flows of dielectric liquid in an annulus" , *J. Mech. Sci. Tech.* 26(12), 3785-3793, 2012.

[39] G. Ahlers, S. Grossmann, D. Lohse, "Heat transfer and large scale dynamics in turbulent Rayleigh-Bénard convection", *Rev. Mod. Phys.,* 81(2), 503, 2009.

[40] P. Traoré, A. T. Pérez, "Two-dimensional numerical analysis of electro-convection in a dielectric liquid subjected to strong unipolar injection", *Phys. Fluid*, 24(3), 037102, 2012.

[41] P. Atten, F. M. J. McCluskey, A. T. Pérez, "Electroconvection and its effect on heat transfer", *IEEE Trans. Electrical Insulation*, 23(4), 659-667, 1988.

Jian Wu (M'13) was born in Jiangxi, China, in 1985. He received the B.Eng. degree in thermal energy and power engineering, the B.B.A. degree in business administration, and the M.Eng. degree in refrigeration and cryogenic engineering from Harbin Institute of Technology (China) in 2006, 2006, and 2008, respectively. He obtained his Ph.D. degree in fluid mechanics from the University of Poitiers, France, in 2012. From 2012 to 2014, he worked as a Research Engineer at PPRIME Institute, University of Poitiers (France). From Nov. 2014 to Jan. 2015, he was as a visiting researcher at University of Seville (Spain). Currently he is working as a Research Engineer at GeoRessources, University of Lorraine (France). His areas of research include electro-hydrodynamics, electro-thermo-hydrodynamics, and computational fluid dynamics. He has coauthored 20 peer-reviewed journal papers and about 20 conference papers. Dr. Wu is a member of IEEE Dielectrics and Electrical Insulation Society and IEEE Industry Applications Society, and a member of European Mechanics Society.

Philippe Traoré was born in Grenoble (France) in September 1963. He graduated from the Superior National Engineer School of Aeronautical Constructions of Toulouse, France in 1987 and received, from University of Toulouse, the Ph.D. degree in fluid mechanics in 1996.

He is currently the deputy director of the mechanical department of the University of Poitiers (France) where he teaches fluid mechanic and scientific computation. His research interests focus on general Computational Fluid Dynamic, two-phase flows, granular media as well as on Electro-hydrodynamic.

Christophe Louste was born in France in 1971. He received the Ph.D. degree from the University of Montpellier II, France in1998. He is working as an associate professor, Dept. of Electronics, at the University of Poitiers France. He joined the Electrofluidodynamic team in 2001. His research interests are electrostatics pumps, electroatomization, and charge production at fluid/solid interfaces. He is a member of the French electrostatic society.

Alberto T. Pérez was born in El Puerto de Santa María Cádiz (Spain) in 1962. He obtained a Bachelor degree from the University of Seville (Spain) in 1985 and a PhD from the same university in 1989.

He is currently Professor at the University of Seville. He has co-authored more than 40 papers on Electro-hydrodynamics, Cohesive Granular Materials and Suspensions in Dielectric Liquids. He was Invited Professor at the Universities of Poitiers (2007 and 2013) and Nice (2008), both in France, and Invited Researcher at the LPMC-CNRS in Nice (2003). He served as Vice Dean of the Faculty of Physics at the University of Seville for 12 years.

Dr. Pérez is member of the American Physical Society.

Pedro A. Vázquez was born in Seville (Spain) in 1969. He received his B.Sc degree from the University of Seville, Spain in 1992, and the Ph.D. degree in Physics from the same university in 1998. He is currently Associate Professor at the Departement of Applied Physics III of the University of Seville, Spain.